Fibers and Polymers 2018, Vol.19, No.8, 1735-1746
DOI 10.1007/s12221-018-8264-2

ISSN 1229-9197 (print version)
ISSN 1875-0052 (electronic version)

Development of Maghemite Glass Fibre Nanocomposite for Adsorptive Removal of Methylene Blue

Muhammad Azeem Ashraf[1,2]*, Jakub Wiener[1], Assad Farooq[2], Jana Saskova[1], and Muhammad Tayyab Noman[1]

[1]*Department of Material Engineering, Technical University of Liberec, Liberec 46117, Czech Republic*
[2]*Department of Fibre and Textile Technology, University of Agriculture, Faisalabad 38040, Pakistan*

(Received April 6, 2018; Revised May 30, 2018; Accepted June 3, 2018)

Abstract: Maghemite glass fibre nanocomposite with excellent magnetic and adsorption properties was successfully developed from nontoxic and eco-friendly reagents by thermal decomposition approach. The developed nanocomposite was utilized in adsorption of methylene blue which follows Freundlich adsorption isotherm. The excellent value of adsorption capacity (51.31 mg g^{-1}) as compared to other adsorbents recommends its potential role for adsorption phenomenon in multiple applications. The developed nanocomposite can be recycled and reused easily. Surface and other functional characteristics of developed nanocomposite were determined through scanning electron microscopy, X-ray diffraction, raman spectroscopy, energy dispersive X-ray spectroscopy and vibrating sample magnetometer. The obtained results revealed that maghemite glass nanocomposite is a potential tool that can be utilized in waste water treatments.

Keywords: Nanocomposite, Maghemite, Adsorption, Wastewater treatment, Methylene blue

Introduction

There is a vast utilization of colours in many industries like textile, paints, cosmetics and printing. Therefore, there are several types of synthetic dyes in wastewater discharging from these industries [1]. As synthetic dyes are non-biodegradable and also destroy photosynthetic activity in water due to blockage of sunlight [2], so these dyes are creating serious problems for aquatic environments. Moreover, in case of human beings, known problems include skin irritation [3], dermatitis and allergy which can cause genetic mutations [4]. Therefore, proper treatment of wastewater to remove dyes and pollutants before discharge is very important.

There are three main categories of methods used for the treatment of dyes wastewater called (i) physical (adsorption and filtration) [5-7], (ii) chemical (electrochemical, oxidation and reduction) [8-10] and (iii) biological (aerobic and anaerobic degradation) [11-14]. Due to capability of treating dyes in various forms [15,16] and ease of design, the adsorption technique is the best substitute as compared to traditional methods of treatment of effluents containing dyes and has been extensively used to remove contaminants from industrial wastewater [17].

There is a dire need for the development of eco-friendly and cheap adsorbents for the adsorption of dyes [18,19]. Recently wastewater treatment by using nanoparticles has increased rapidly because of their reactivity and high surface area [20-26]. Because of high adsorption capacity, activated carbon is used in commercial systems for elimination of different dyes [27-29], but due to high cost its usage is limited [30,31]. Conventional and cheap adsorbents have some drawbacks e.g. they are difficult to separate from the solution and their recycling is not easy. Also nanoparticles used for adsorption of dyes can aggregate during the dye removal process.

Recently having high adsorption capacity and chemical stability, nano adsorbents containing iron have gained much attention [32-35] due to lower cost as compared to activated carbon [36]. Technological applications of multifunctional textiles have gained much interest over past decades [37-41]. Integration of magnetic nanoparticles with textiles have produced new characteristics including electromagnetic wave shielding and magnetism [42,43]. Intelligent textile materials having magnetic properties can be used for magnetic filters, bio-sensors and magneto graphic printing [44]. Intensive work has been carried out on iron containing nanomaterials like maghemite (γ-Fe_2O_3), magnetite (Fe_3O_4) and hematite (α-Fe_2O_3). Many procedures have been reported for their synthesis among which co precipitation and thermal decomposition methods are considered as most suitable and low cost [45,46]. Due to distinctive characteristics, iron containing nanomaterials have been used in many biomedical applications such as hyperthermia for therapy, bio-separation and target delivery of drugs for treatment of cancer [47-50].

Application of iron containing nanomaterials on textile materials has been limited to the coating of Fe_3O_4 nanoparticles synthesised by a hydrothermal method on polyamide 6 fibres (PA 6). Immobilization of magnetite nanoparticles on the PA 6 fabric was reported by using ferrous chloride, ferric trichloride as the precursors and sodium dodecyl sulfate as dispersing agent [51]. Furthermore, some fibres were prepared by integrating magnetic nanoparticles during the fibre manufacturing process [52,53].

Generally two methods can be used to prepare magnetic fibres which include synthesis on the surface and filling with magnetic particles in the lumen. In lumen filling process,

*Corresponding author: azeemashraf786@hotmail.com

maghemite or magnetite nanoparticles can be inserted into fibre's lumen to produce the magnetic paper [54-58]. Due to having large lumen, kenaf fibres were used to prepare magnetic paper by co-precipitation method by using ferric and ferrous compounds. Further, the effects of processing parameters on particle size, magnetic properties and thermal stability were observed [59]. In case of in situ synthesis method magnetite nanoparticles can be synthesised with co-precipitation by oxidation of ferrous hydroxide and deposited into the fibre's lumen [60-71]. However, no significant study was reported in literature until now associated to the manufacture of magnetic maghemite glass nanocomposite (MGN) by thermal decomposition method.

In this research work, thermal decomposition route was used for the development of magnetic maghemite glass nanocomposite. MGN was successfully synthesised by using ferric nitrate, urea and nonwoven glass fibre mat. The surface morphology, chemical structure and magnetic properties were determined by different characterization techniques. The synthesised nanocomposite was utilized to efficiently adsorb methylene blue (MB) dye.

Experimental

Materials

Reagents used in this research work i.e. Ferric Nitrate [$Fe(NO_3)_3 \cdot 9H_2O$], Urea (CH_4N_2O) were received from Sigma Aldrich. No further purification of reagents was carried out. Non-woven glass fibre mat created from E-glass formulation having specifications [72] as listed in Table 1 was obtained from Spepat s.r.o. Roudnice nad Labem, Czech Republic. Because the normal fabrics from natural fibres can be degraded at higher temperatures so they cannot be used efficiently as substrate for synthesis of iron oxide nanoparticles by thermal decomposition method. The glass fibre mat was selected due to its thermal stability at very high temperatures.

Table 1. Glass fibre mat specifications

Properties	Value
Surface weight (g m^{-2})	270
Thickness (mm)	1.6
Breaking length (m)	260
Tensile strength (N)	26.60

Methylene blue dye of molecular weight 319.85 g mol^{-1} used in this research work for adsorption experiments was obtained from Sigma Aldrich. Methylene blue dye was selected as model pollutant as it is most widely used in literature for adsorption experiments.

Synthesis of Nanocomposite

Maghemite glass nanocomposite was synthesised at optimized conditions. Solutions of ferric nitrate $Fe(NO_3)_3 \cdot 9H_2O$ and urea CH_4N_2O were mixed together with molar ratio of 1:6 and agitated for 10 min to get a uniform mixture. This solution was poured on glass fibre mat then it was placed in high temperature furnace and treated for 30 min at 300 °C with 10 °C min^{-1} heating rate. After 30 min, samples were cooled down at the same rate. The schematic representation for the synthesis of maghemite glass nanocomposite is illustrated in Figure 1.

Test Methods

Surface characteristics of maghemite glass nanocomposite were analysed by ultra-high resolution scanning electron microscope (SEM, Carl Zeiss Meditec AG, Germany). Elemental analysis of samples was carried out by energy dispersive X-ray spectrometer (EDS, JEOL Ltd., Tokyo, Japan) for detection of maghemite nanoparticles. X-ray diffractometer (PANanlytical BV Almelo, Netherlands) with Cu-Kα radiation was employed for recording the XRD patterns. Raman spectroscopy was done with Raman

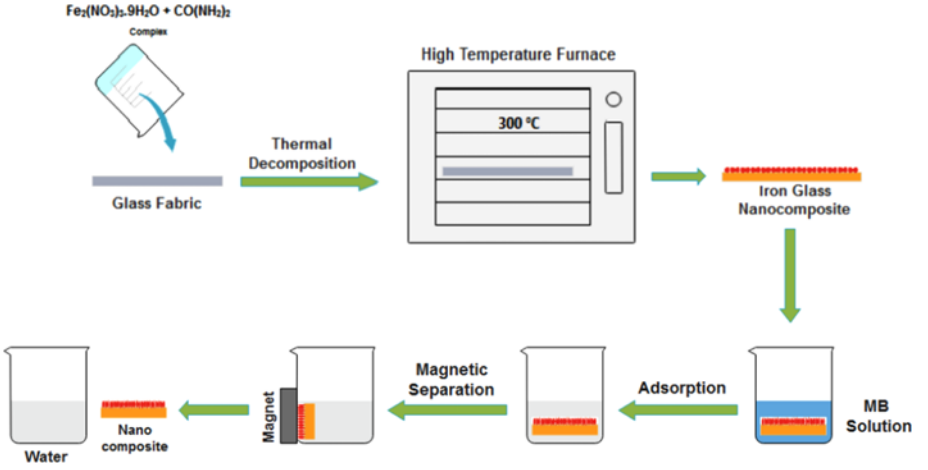

Figure 1. Graphical representation for synthesis of maghemite glass nanocomposite for methylene blue adsorption.

Microscope DXR from Thermoscientific. Magnetic properties were recorded at room temperature on vibrating sample magnetometer (VSM, Lake Shore 7407). The magnetic attraction of the MGN was observed with the help of a strong magnet.

Adsorption of Methylene Blue on Maghemite Glass Nanocomposite

To examine methylene blue adsorption by MGN, different solutions of MB dye in distilled water were prepared having concentration from 50 to 90 mg l^{-1}. Higher concentration levels of methylene blue dye were selected to simulate real dyeing wastewater as the industrial dyeing wastewater contain high amounts of dyes. To find the equilibrium point, 1.25 g l^{-1} adsorbent was added to MB solution at pH 8. The solution was agitated for 150 minutes at 30 °C temperature with agitation speed of 200 rpm. The impact of adsorbent amount was investigated by changing adsorbent quantity from 0.25 to 1.25 g l^{-1}. To investigate the influence of stirring, the agitation was changed from 50 to 200 rpm by using GFL Analogue Orbital Shaker 3005. Solution temperatures were adjusted to 30 °C, 40 °C and 50 °C to find the impact of temperature on adsorption. The alteration in pH was done from 2 to 10 to check the impact of pH. The pH of solutions was adjusted by using suitable amounts of HCl or NaOH. Solid addition method was used to determine the point of zero charge as reported in literature [73]. Dye removal was determined with assistance of UV-Visible spectrometer (UV-1600PC Spectrophotometer, VWR International) by analysing the solution after fixed intervals of time.

Dye removal percentage from solution was determined with the help of equation (1).

$$R(\%) = \frac{(C_0 - C_t)}{C_0} \times 100 \tag{1}$$

Adsorption capacity was calculated by equation (2) at any time *t*.

$$q_t = \frac{(C_0 - C_t)V}{m} \tag{2}$$

where C_0 (mg l^{-1}) is initial concentration of dye in solution, C_t (mg l^{-1}) is dye concentration at time t (min), m (g) is adsorbent mass and V (l) is solution volume.

Adsorption Isotherms

Langmuir and Freundlich isotherms were used to explain the adsorption mechanism of MB by MGN. The nonlinear form of Langmuir model [74] is expressed in equation (3).

$$q_e = \frac{q_m K_L C_e}{1 + K_L C_e} \tag{3}$$

The Langmuir isotherm in linear form is expressed as in equation (4).

$$\frac{C_e}{q_e} = \frac{1}{q_m K_L} + \frac{C_e}{q_m} \tag{4}$$

where C_e (mg l^{-1}) is dye concentration at equilibrium in solution, q_e (mg g^{-1}) is the dye amount which adsorbed at equilibrium on adsorbent, q_m (mg g^{-1}) shows maximum adsorption capacity and K_L (l mg^{-1}) represents Langmuir constant.

Freundlich isotherm model [75] is expressed in equation (5).

$$q_e = K_F C_e^{1/n} \tag{5}$$

After linearizing Freundlich equation can be written in equation (6).

$$\log(q_e) = \log(K_F) + \frac{1}{n}\log(C_e) \tag{6}$$

Here K_F is Freundlich constant (mg g^{-1}) (l mg^{-1})$^{1/n}$ and $1/n$ is Freundlich constant expressing intensity of adsorption.

Adsorption Kinetics

Rate constant and adsorption order can be realized with adsorption kinetics. Pseudo first order and pseudo second order models were used to study the adsorption kinetics of MB on MGN.

The pseudo first order kinetics model [76] is described in equation (7):

$$q_t = q_e(1 - e^{-K_1 t}) \tag{7}$$

where K_1 is rate constant for first order kinetics (min^{-1}), q_t and q_e are the dye amounts (mg g^{-1}) adsorbed at any time t (min) and at equilibrium respectively.

Pseudo first order kinetics model in its linear form can be described in equation (8).

$$\log(q_e - q_t) = \log(q_e) - \frac{K_1 t}{2.303} \tag{8}$$

Pseudo second order kinetics model equation [77] can be expressed as in equation (9).

$$q_t = \frac{q_e^2 K_2 t}{(1 + q_e K_2 t)} \tag{9}$$

where K_2 is the rate constant for pseudo second order kinetics (g mg^{-1} min^{-1}).

The linear form of pseudo second order model [78,79] is expressed in equation (10).

$$\frac{t}{q_t} = \frac{2}{K_2 q_e^2} + \frac{t}{q_e} \tag{10}$$

Adsorption Thermodynamics

Methylene blue adsorption thermodynamics were

investigated by following equations.

$$\Delta G^{o} = -RT\ln K_c \quad (11)$$

where ΔG^{o} (kJ mol^{-1}) is Gibb's free energy, R is gas constant (8.314 J mol^{-1} K^{-1}), T is temperature (K) and K_c (Dimensionless) is thermodynamic constant.

The relationship between the thermodynamic parameters is described as in equation (12).

$$\Delta G^{o} = \Delta H^{o} - T\Delta S^{o} \quad (12)$$

where, ΔS^{o} (J mol^{-1}) is entropy and ΔH^{o} (kJ mol^{-1}) is enthalpy.

By substituting equation (11) into equation (12) the Van't Hoff equation is obtained.

$$\ln K_c = \frac{-\Delta H^{o}}{RT} + \frac{\Delta S^{o}}{R} \quad (13)$$

K_c is thermodynamic constant which is a dimensionless quantity and can be obtained by multiplying Langmuir constant (K_L, l mg^{-1}) by 10^6 [80,81]. Accurate determination of equilibrium constant (K_c) is very important for correct calculation of parameters [82].

ΔG^{o} values were determined from equation (11) while ΔH^{o} and ΔS^{o} values were determined by the slope and intercept of plot of $\ln K_c$ against $1/T$ respectively (equation (13)).

Stability and Reusability

To investigate the stability of synthesized MGN adsorbent, the leaching of iron ions was measured by adding 250 mg adsorbent in 200 ml water. The blend was stirred for 150 minutes at 200 rpm speed and pH was changed from 2 to 10. The iron ions leached in water were analysed with Inductively Coupled Plasma (ICP-AES) analysis.

Recycling and reusability of the developed MGN adsorbent was evaluated by ten consecutive cycles of adsorption and desorption. For desorption, dye loaded adsorbent was dispersed in 200 ml water at pH 2 and shaken for 60 minutes. After desorption, magnetic MGN was recovered by magnetic separation from solution and dried for 60 minutes at 90 ^{o}C.

Results and Discussion

SEM Analysis

High magnification images from SEM of the synthesised MGN are presented in Figure 2(a-d). The maghemite nanoparticles were incorporated into the glass structure. Average size of maghemite nanoparticles observed to be nearly 20 nm. The resultant nanoparticles are mostly spherical and evenly distributed.

Energy Dispersive Spectroscopy (EDS) Analysis

Successful synthesis of iron oxide (maghemite) nanoparticles on maghemite glass nanocomposite was confirmed by EDS

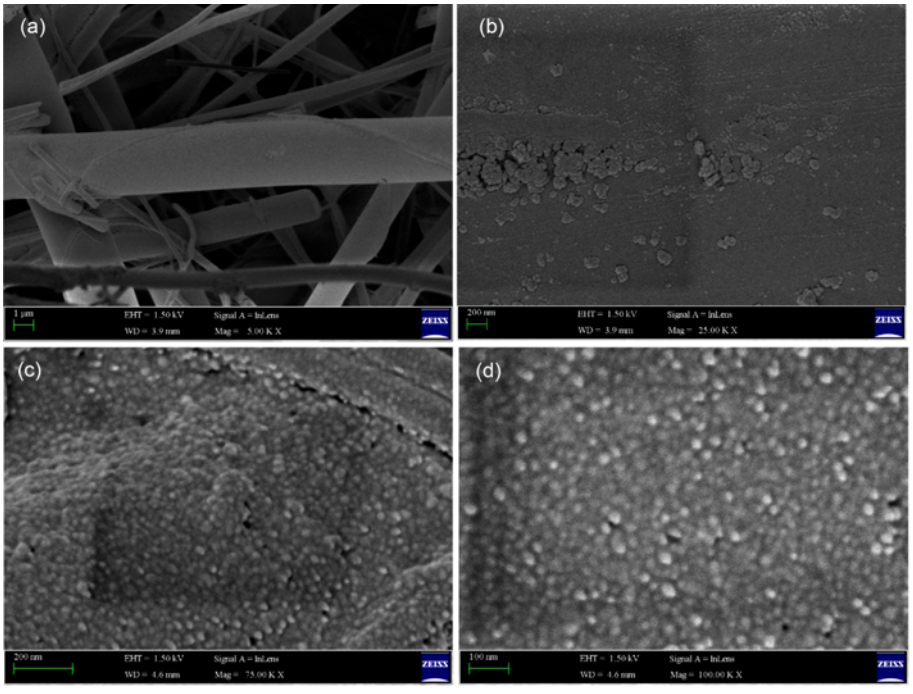

Figure 2. SEM images of maghemite glass nanocomposite; (a) magnification 5 K, (b) magnification 25 K, (c) magnification 75 K, and (d) magnification 100 K.

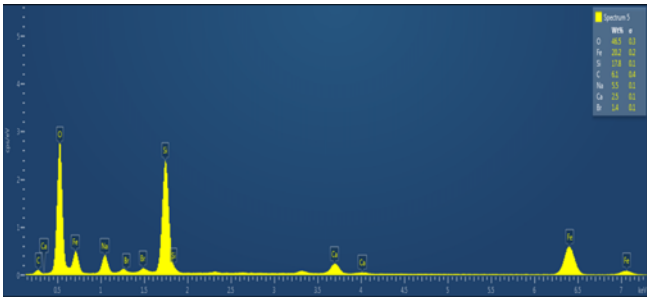

Figure 3. EDS spectra of maghemite glass nanocomposite.

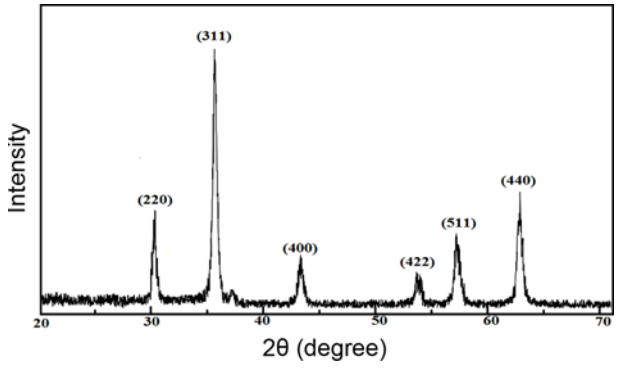

Figure 4. XRD pattern of maghemite glass nanocomposite.

analysis. The results in Figure 3 show peaks of Fe, Si and O.

XRD Analysis

The XRD diffraction patterns acquired by using PANanlytical BV Almelo, Netherlands X-ray diffractometer are presented in Figure 4. The XRD diffraction peaks (220), (311), (400), (422), (511) and (440) indexed to the cubic spinel structure (JCPDS No. 39-1346) shows the formation of pure maghemite [83-85]. The strong XRD peaks revealed the well crystalized structure of maghemite [86].

The crystal size of maghemite nanoparticles was found to be 20 nm by using Scherer's equation (14).

$$D = \frac{K\lambda}{(b\cos\theta)} \tag{14}$$

The smaller size of maghemite nanoparticles may be due to attachment of particles with surface of the glass which obstruct the progression of as synthesised nanoparticles.

Raman Spectroscopy

To further verify the formation of pure maghemite, Raman spectroscopy was utilized. Raman spectra of as synthesized nanocomposite is presented in Figure 5. Broad bands around 350, 500, 670 and 1330 cm^{-1} confirms the formation of pure maghemite. These bands are characteristic of maghemite and not present in spectrum of other iron oxides [87,88].

Magnetic Properties

The graphical representation of magnetic hysteresis loop

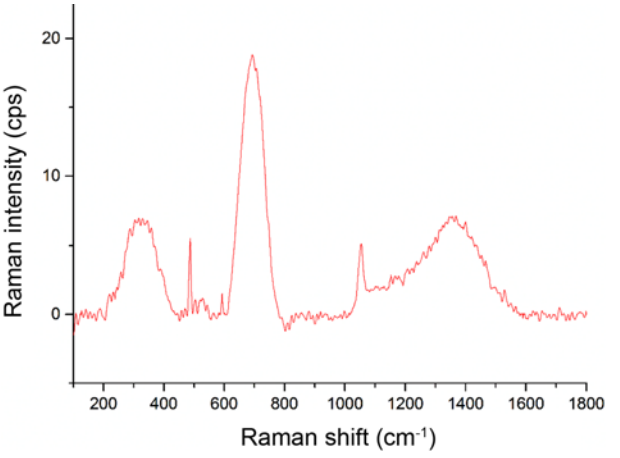

Figure 5. Raman spectra of maghemite glass nanocomposite.

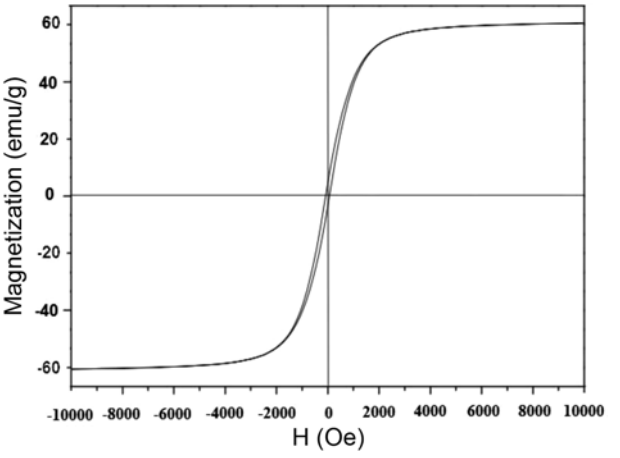

Figure 6. Magnetization hysteresis curves of maghemite glass nanocomposite.

of MGN measured by using VSM is presented in Figure 6. The magnetic saturation of MGN found to be 60 emu g^{-1} with 7 emu g^{-1} remanent magnetization. The saturation magnetization is lower than that of bulk maghemite crystallite (i.e., 73.5 emu/g). This difference has also been reported by other investigators [89,90], and it is probably due to the surface spin canting effects [91]. The magnetic properties of ferromagnetic materials depends on their nature and surface morphology. The sensitivity of MGN was confirmed by attraction towards a magnet.

Adsorption of Methylene Blue by Maghemite Glass Nanocomposite

Effect of Dye Concentration

The amount of MB dye was varied from 50 mg l^{-1} to 90 mg l^{-1} to study the effect of dye initial concentration on adsorption behaviour of MB on MGN while other process conditions were fixed at pH 8, adsorbent dosage 1.25 g l^{-1}, agitation speed 200 rpm and temperature 30 °C. It was

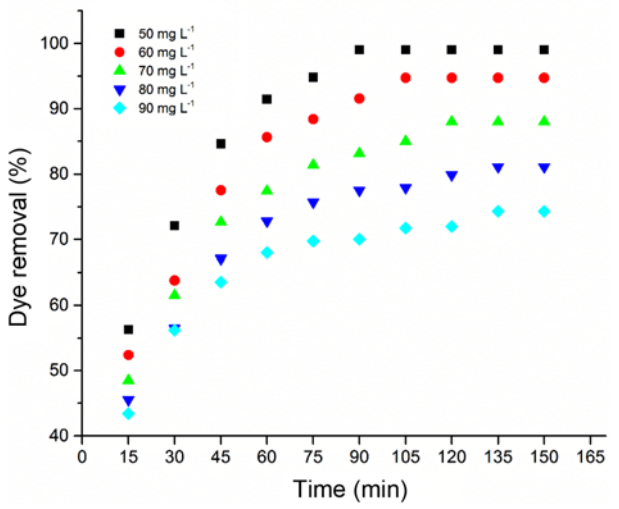

Figure 7. Effect of dye initial concentration on removal percentage.

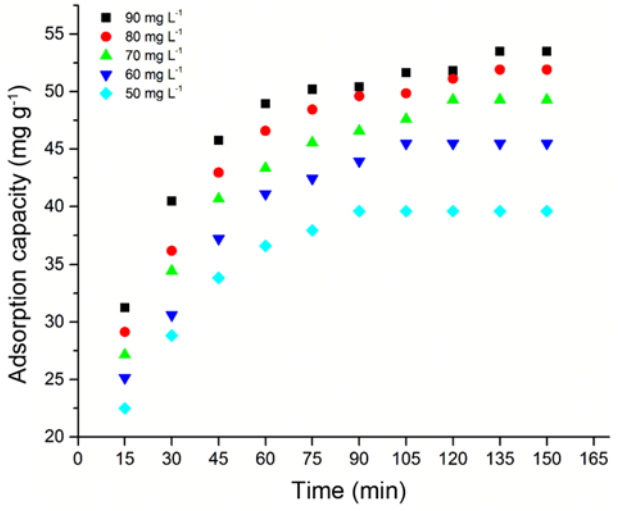

Figure 8. Effect of dye initial concentration on adsorption capacity.

observed that by increasing dye concentration, removal percentage decreased and maximum removal percentage of 99 % was observed with 50 mg l^{-1}. The decrease in removal percentage may be due to the saturation of adoption sites at higher dye concentration levels. By increasing dye concentration it took more time to attain the equilibrium point as shown in Figure 7. The availability of relative higher number of adsorption sites at low concentration of dye may cause the lower equilibrium time. Equilibrium was attained in 90 minutes for 50 mg l^{-1} while it took 130 minutes to attain equilibrium for 90 mg l^{-1}.

Adsorption capacity enhanced by increasing dye concentration as shown in Figure 8. This behaviour is because of the availability of more molecules of dye per unit quantity of

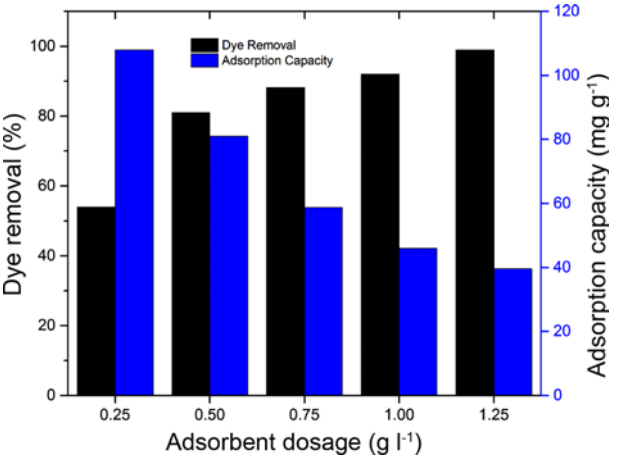

Figure 9. Effect of adsorbent dosage on dye adsorption.

adsorbent. Dye initial concentration would deliver a driving force to overtake the mass transfer resistance so the adsorption capacity enhanced by increasing dye initial concentration. These outcomes are according to the findings of previous investigators [92-94] who reported that MB removal percentage increased by decreasing dye initial concentration while adsorption capacity decreased which shows that dye removal efficiency depends on concentration.

Effect of Adsorbent Dosage

The quantity of MGN adsorbent was changed from 0.25 g l^{-1} to 1.25 g l^{-1} to investigate the impact of adsorbent amount on removal percentage and capacity. MB concentration was 50 mg l^{-1}, temperature 30 °C, pH 8, contact time 150 min and agitation speed 200 rpm. An increasing trend in dye removal percentage and a decreasing trend in adsorption capacity can be noted by increasing adsorbent dosage as illustrated in Figure 9.

With adsorbent 0.25 g l^{-1} the dye removal efficiency was 54 % which increased to 81 %, 88.2 %, 92 % and 99 % with increase of the adsorbent amount to 0.50 g l^{-1}, 0.75 g l^{-1}, 1 g l^{-1} and 1.25 g l^{-1} respectively. By increasing adsorbent amount, the availability of higher number of adsorption sites results in the increase in removal percentage of dye. Removal percentage was increased by increasing the amount of adsorbent but adsorption capacity decreased at the same time. This happened due to aggregation or unsaturation of the adsorbent active sites at higher amounts of adsorbent [95].

Effect of pH

The pH shows very significant effect for MB adsorption by MGN. The effect of pH was determined by varying pH from 2 to 10 at dye initial concentration 50 mg l^{-1}, adsorbent dosage 1.25 g l^{-1}, agitation speed 200 rpm and temperature 30 °C. It is clear from Figure 10 that by increasing pH, both removal percentage and adsorption capacity increased due to the increased negative charge on adsorbent surface. On the other hand by decrease in the pH, there is a growth of

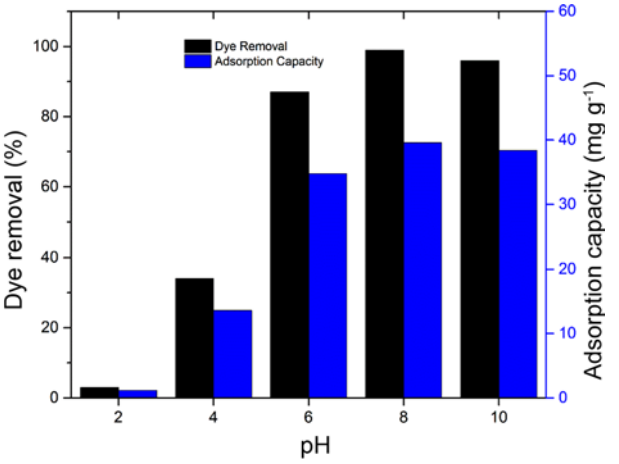

Figure 10. Effect of pH on dye adsorption.

positive charge on the surface of adsorbent as a number of positive (H^+) ions gathered on the adsorbent from bulk solution. Consequently, dye removal efficiency decreased by decreasing the pH from point of zero charge. The build-up of H^+ ions on nanocomposite surface makes the interaction of positively charged dye molecules more difficult. Dye removal was negligible at lower pH value of 2. Removal percentage increased significantly by increasing the pH above the zero charge point. Highest results for dye removal were obtained at pH of 8 because of the increased attraction between negatively charged nanocomposite and positively charged dye molecules.

Effect of Agitation Speed

Agitation impact was investigated by changing the speed from 50 rpm to 200 rpm by keeping other parameters at 1.25 g l^{-1} adsorbent dosage, pH 8, temperature 30 ^{o}C and dye concentration of 50 mg l^{-1}. One sample was investigated without any agitation for reference. It can be observed from the Figure 11 that only 28 % dye from solution was removed

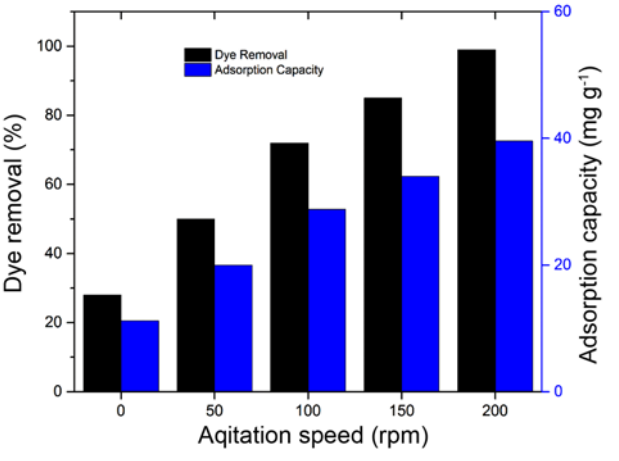

Figure 11. Effect of agitation speed on dye adsorption.

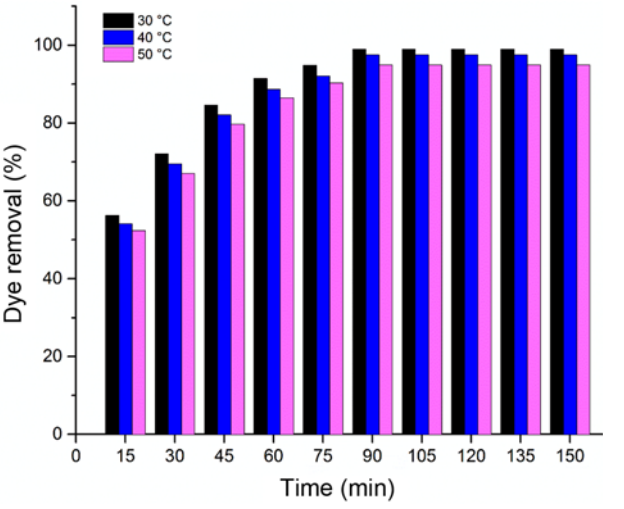

Figure 12. Effect of temperature on dye removal.

without agitation however, dye removal efficiency was 50 %, 72 %, 85 % and 99 % at 50, 100, 150 and 200 rpm respectively. With the increase of agitation speed a rise in adsorption capacity was noted. This happened because agitation increases the interactions between adsorbent and methylene blue dye.

Effect of Temperature

Solution temperatures were adjusted from 30 to 50 ^{o}C to explore temperature impact on removal of dye by MGN while keeping other parameters at adsorbent dosage 1.25 g l^{-1}, dye initial concentration 50 mg l^{-1}, pH 8 and agitation speed of 200 rpm.

By increasing solution temperature there is a small decrease in dye removal efficiency as shown in Figure 12. This drop in dye removal indicates that MB adsorption on MGN is less favourable at higher temperatures. Mobility of dye molecules increased by increasing temperature which may cause the escape of adsorbed dye molecules from the adsorbent to solution. Therefore, the adsorption capacity decreased by increasing temperature.

Adsorption Isotherms

Adsorption isotherms study describes the interaction of an adsorbate and adsorbent. Adsorption isotherm explains association between quantity of dye adsorbed on adsorbent and dye concentration in solution at equilibrium. Langmuir isotherm considers that the adsorption is homogeneous and monolayer due to uniform availability of sites for adsorption having even adsorbate affinity. Freundlich isotherm consider that the nature of adsorbent is heterogeneous with uneven distribution of functional groups.

The Langmuir and Freundlich isotherms of nonlinear form were drawn with the help of OriginPro 9 software from OriginLab Corporation by plotting C_e and q_e as presented in Figure 13.

The parameters of Langmuir and Freundlich isotherm

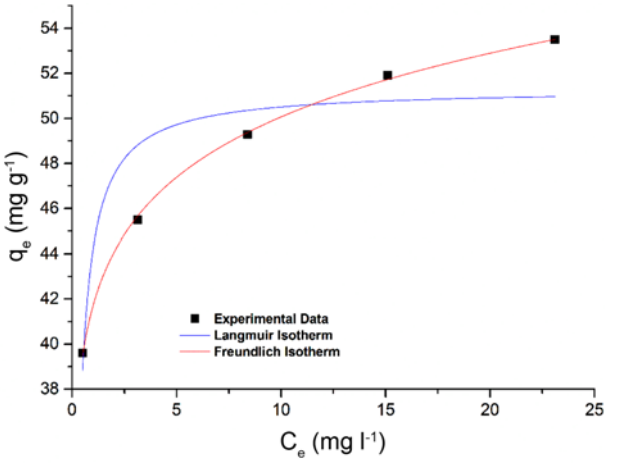

Figure 13. Adsorption isotherms (a) Langmuir (b) Freundlich for adsorption of MB on maghemite glass nanocomposite at 30 °C.

Table 2. Langmuir and Freundlich isotherm parameters for the adsorption of methylene blue

Langmuir			Freundlich		
q_{max} (mg g^{-1})	K_L (l mg^{-1})	R^2	K_F (mg g^{-1}) (l mg^{-1})$^{1/n}$	$1/n$	R^2
51.31	6.2066	0.8334	41.70	0.07	0.9992

obtained by nonlinear regression are presented in Table 2. Maximum adsorption capacity (q_{max}) obtained by Langmuir model is 51.31 mg g^{-1}. It was observed from results that Langmuir isotherm could not fully describe the methylene blue adsorption. The R^2 values of 0.8334 and 0.9992 were found for Langmuir and Freundlich models respectively for MB adsorption on MGN. The higher R^2 for Freundlich isotherm shows the better fitness of the model as compared to Langmuir. It may be due to morphology of MGN and heterogeneous distribution of maghemite nanoparticles on glass surface.

Separation factor R_L is an important parameter based on Langmuir model as described by the Hall *et al.* [96] and is presented in equation (15).

$$R_L = \frac{1}{1+K_L C_0} \quad (15)$$

where C_0 is the dye initial concentration and K_L is the Langmuir constant.

R_L is used to describe the feasibility of adsorption on adsorbent. The R_L value determines the type of adsorption as follows:

linear ($R_L = 1$),
favourable ($0 < R_L < 1$)
unfavourable ($R_L > 1$)
irreversible ($R_L = 0$)

The calculated R_L values were in the range of 0.0032 to 0.0017 which falls in the category of between 0 and 1 for different initial dye concentrations which confirms that adsorption of methylene blue on iron glass nanocomposite is favourable.

Adsorption Kinetics

Pseudo first order and pseudo second order models were

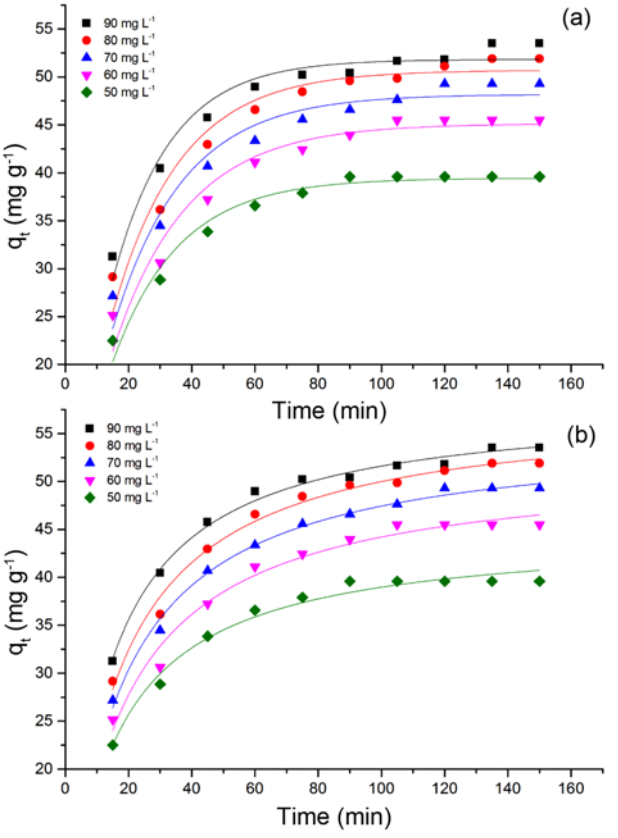

Figure 14. Adsorption kinetics of methylene blue (a) Pseudo first order kinetics and (b) Pseudo second order kinetics.

Table 3. Parameters of pseudo first order and pseudo second order models

Kinetic model parameters	Initial concentration (mg l^{-1})				
	50	60	70	80	90
q_e, exp (mg g^{-1})	39.60	45.48	49.28	51.90	53.50
Pseudo first order					
q_e, cal (mg g^{-1})	39.43	45.11	48.17	50.68	51.81
K_1 (min^{-1})	0.0481	0.0428	0.0452	0.0464	0.0541
R^2	0.9700	0.9504	0.9513	0.9514	0.9598
Pseudo second order					
q_e, cal (mg g^{-1})	44.73	51.89	55.18	57.80	58.13
K_2 (min^{-1})	0.0015	0.0011	0.0011	0.0011	0.0013
R^2	0.9823	0.9791	0.9938	0.9892	0.9941

Table 4. Adsorption thermodynamic parameters

T (K)	K_c	ΔG^o (kJ mol^{-1})	ΔH^o (kJ mol^{-1})	ΔS^o (J mol^{-1})
303	6210,000	-39.40		
313	2120,000	-37.92	-62.33	-76.49
323	1350,000	-37.92		

plotted to determine kinetics of MB dye adsorption on MGN. Time was taken on X-axis while q_t was taken on Y-axis to plot the nonlinear models as presented in Figure 14.

The kinetic parameter of both models are presented in Table 3 which are calculated by the nonlinear regression. The q_e calculated values for pseudo first order model are near to the experimental values (q_e, exp) while in case of second order model the R^2 values are greater than those of pseudo first order model. Therefore, methylene blue dye adsorption on MGN follows pseudo second order model.

Adsorption Thermodynamics

Thermodynamics parameter for the adsorption of MB by MGN adsorbent are listed in Table 4. The degree of spontaneity of process can be determined by Gibb's energy change (ΔG^o). Adsorption process will be more spontaneous if sign of ΔG^o is negative. The negative ΔG^o values shows that MB adsorption by MGN is spontaneous.

Negative values of ΔH^o ($\Delta H^o<0$) for adsorption of MB by MGN shows the exothermic nature of adsorption. This exothermic nature shows the release of energy during the adsorption process. This implies decrease in equilibrium constant (K_c) and adsorption capacity (q_e) by increasing temperature.

Further the sign and magnitude of ΔS^o determine the organization of adsorbate molecules at adsorbent interface. The ΔS^o value is negative which shows less random organization of dye molecules at adsorbent interface during MB adsorption by MGN. Thermodynamic parameters shows that MB adsorption on MGN involves physical adsorption.

Stability of Adsorbent

As the leakage of metal ions in water from adsorbent is unacceptable so the stability of nanocomposite was assessed at different pH levels. The concentration of iron ions is 3 mg l^{-1} at pH 2, while at pH levels higher than 2 leaching of iron is negligible as shown in Figure 15. Similar results were reported in previous studies from iron containing composites [97-100]. These results shows the stability of synthesized nanocomposite at vast range of pH levels which is useful for treating wastewater.

Recycling and Reusability

Reusability is an important characteristic of any adsorbent to be used efficiently for dye removal. To evaluate the reusability of MGN for dye removal ten consecutive adsorption and desorption cycles were performed. MGN

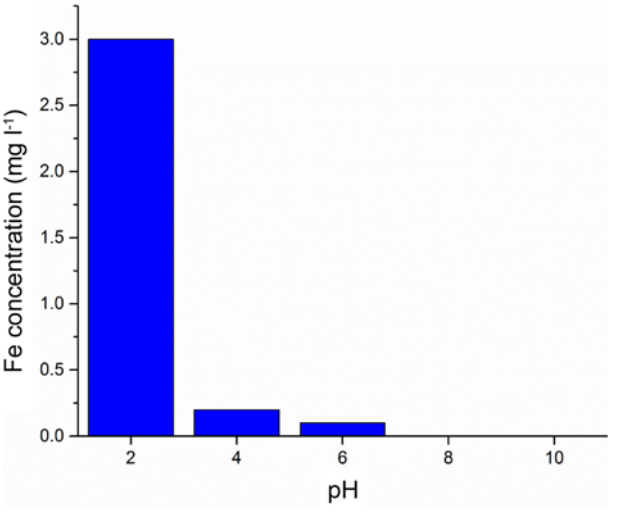

Figure 15. Leaching of iron at different pH levels.

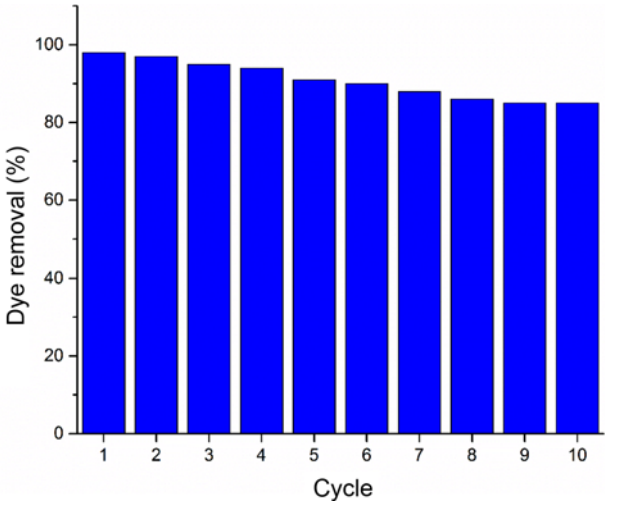

Figure 16. Dye removal efficiency of maghemite glass nanocomposite for 10 cycles.

Table 5. Comparison of methylene blue adsorption by various adsorbents

Adsorbent	q_m (mg g^{-1})	Reference
Activated carbon from coir	14.36	[101]
Activated carbon from ficus carica	47.62	[102]
Activated carbon from olive stone	16.12	[103]
Iron impregnated activated carbon	20.61	[104]
Activated carbon from acrylic	8.76	[105]
Carbon nanotube nanocomposite	15.87	[106]
Magnetite powder	20.74	[107]
M-MWCNTs	48.06	[73]
MnP	25.54	[108]
Maghemite glass nanocomposite	51.31	Present work

exhibits good removal efficiency of 87 % even after 10 cycles as shown in Figure 16. This indicates good performance of nanocomposite for dyes removal from wastewater.

Adsorption Comparison

Maximum adsorption capacity of various adsorbents to remove MB is shown in Table 5 for comparison. The adsorption of MGN is higher than many previously reported adsorbents which shows its great potential for dyes adsorption from water.

Conclusion

In this work an economical strategy was developed for the fabrication of maghemite glass nanocomposite. The method described here for fabrication of MGN is eco-friendly, cost effective and indicates potential for large scale production. The dye adsorption efficiency of synthesised nanocomposite was investigated by adsorption of MB. The calculated adsorption capacity of synthesised MGN was 51.31 mg g^{-1}. Further the effect of different important processing parameters was evaluated on adsorption of MB by MGN. The MB dye adsorption on MGN follows Freundlich isotherm model with R^2 value of 0.9992. It was observed that MB adsorption on MGN follows pseudo second order model. The MGN exhibited excellent stability and recycling even after ten cycles of use which indicates that MGN adsorbent can be employed efficiently for removal of MB from wastewater.

References

1. P. Sharma, H. Kaur, M. Sharma, and V. Sahore, *Environ. Monit. Assess.*, **183**, 151 (2011).
2. B. Balci, O. Keskinkan, and M. Avci, *Expert Syst. Appl.*, **38**, 949 (2011).
3. D. S. Brookstein, *Derm. Clin.*, **27**, 309 (2009).
4. P. A. Carneiro, G. A. Umbuzeiro, D. P. Oliveira, and M. V. B. Zanoni, *J. Hazard. Mater.*, **174**, 694 (2010).
5. A. Afkhami and R. Moosavi, *J. Hazard. Mater.*, **174**, 398 (2010).
6. N. Kannan and M. M. Sundaram, *Dyes Pigm.*, **51**, 25 (2001).
7. S. Wang, H. Li, and L. Xu, *J. Colloid Interface Sci.*, **295**, 71 (2006).
8. I. Arslan and I. A. Balcioglu, *Color. Technol.*, **117**, 38 (2001).
9. M. Gutierrez, M. Pepió, and M. Crespi, *Color. Technol.*, **118**, 1 (2002).
10. S. Tsui and W. Chu, *Water Sci. Technol.*, **44**, 173 (2001).
11. J. Bell and C. A. Buckley, *Water SA*, **29**, 129 (2003).
12. M. R. Haghighi-Podeh, M. Sarhadi, and S. M. Ghoreyshi, *Water Qual. Res. J. Can.*, **36**, 605 (2001).
13. I. K. Kapdan and R. Ozturk, *J. Hazard. Mater.*, **123**, 217 (2005).
14. A. Stolz, *Appl. Microbiol. Biotechnol.*, **56**, 69 (2001).
15. K. M. Doke and E. M. Khan, *Rev. Environ. Sci. Biotechnol.*, **12**, 25 (2013).
16. M. Sharma, R. K. Vyas, and K. Singh, *Adsorption*, **19**, 161 (2013).
17. L. Wang and J. Li, *Ind. Crops Prod.*, **42**, 153 (2013).
18. A.-F. Ngomsik, A. Bee, M. Draye, G. Cote, and V. Cabuil, *Comptes Rendus Chimie*, **8**, 963 (2005).
19. P. G. Tratnyek and R. L. Johnson, *Nano Today*, **1**, 44 (2006).
20. M. S. Diallo and N. Savage, *J. Nanopart. Res.*, **7**, 325 (2005).
21. M. M. Husein, L. Patruyo, P. Pereira-Almao, and N. N. Nassar, *J. Colloid Interface Sci.*, **342**, 253 (2010).
22. N. N. Nassar and M. M. Husein, *Fuel Process. Technol.*, **91**, 164 (2010).
23. N. N. Nassar, M. M. Husein, and P. Pereira-Almao, *Fuel Process. Technol.*, **91**, 169 (2010).
24. N. Savage and M. S. Diallo, *J. Nanopart. Res.*, **7**, 331 (2005).
25. G. A. Waychunas, C. S. Kim, and J. F. Banfield, *J. Nanopart. Res.*, **7**, 409 (2005).
26. Z. Yue and J. Economy, *J. Nanopart. Res.*, **7**, 477 (2005).
27. A. Afkhami, T. Madrakian, A. Amini, and Z. Karimi, *J. Hazard. Mater.*, **150**, 408 (2008).
28. A. Afkhami, T. Madrakian, Z. Karimi, and A. Amini, *Colloid Surf. A-Physicochem. Eng. Asp.*, **304**, 36 (2007).
29. L. C. Oliveira, R. V. Rios, J. D. Fabris, V. Garg, K. Sapag, and R. M. Lago, *Carbon*, **40**, 2177 (2002).
30. J. M. Dias, M. C. Alvim-Ferraz, M. F. Almeida, J. Rivera-Utrilla, and M. Sánchez-Polo, *J. Environ. Manage.*, **85**, 833 (2007).
31. A. Ip, J. Barford, and G. McKay, *Bioresour. Technol.*, **99**, 8909 (2008).
32. I. Ahmed and M. Gasser, *Appl. Surf. Sci.*, **259**, 650 (2012).
33. E. Rosales, O. Iglesias, M. Pazos, and M. Sanromán, *J. Hazard. Mater.*, **213**, 369 (2012).
34. J. Trujillo-Reyes, M. Solache-Ríos, A. R. Vilchis-Nestor, V. Sánchez-Mendieta, and A. Colín-Cruz, *Water, Air, & Soil Pollution*, **223**, 1331 (2012).
35. L. Zhou, J. Jin, Z. Liu, X. Liang, and C. Shang, *J. Hazard. Mater.*, **185**, 1045 (2011).
36. S. Pirillo, M. L. Ferreira, and E. H. Rueda, *Ind. Eng. Chem. Prod. Res.*, **46**, 8255 (2007).
37. Y. Liu, J. Tang, R. Wang, H. Lu, L. Li, Y. Kong, K. Qi, and J. Xin, *J. Mater. Chem.*, **17**, 1071 (2007).
38. Y. Boguslavsky, T. Fadida, Y. Talyosef, and J.-P. Lellouche, *J. Mater. Chem.*, **21**, 10304 (2011).
39. M. Montazer and V. Allahyarzadeh, *Ind. Eng. Chem. Prod. Res.*, **52**, 8436 (2013).
40. I. Perelshtein, E. Ruderman, N. Perkas, T. Tzanov, J. Beddow, E. Joyce, T. J. Mason, M. Blanes, K. Mollá, and A. Patlolla, *J. Mater. Chem. B*, **1**, 1968 (2013).

41. L. Wu, J. Zhang, B. Li, and A. Wang, *J. Mater. Chem. B*, **1**, 4756 (2013).
42. D. Fragouli, I. S. Bayer, R. Di Corato, R. Brescia, G. Bertoni, C. Innocenti, D. Gatteschi, T. Pellegrino, R. Cingolani, and A. Athanassiou, *J. Mater. Chem.*, **22**, 1662 (2012).
43. J. Zieba and M. Frydrysiak, *Smar. Res. J.*, **1**, 102 (2012).
44. M. Rubacha and J. Zięba, *Fibres Text. East. Eur.*, **14**, 49 (2006).
45. X.-L. Fang, C. Chen, M.-S. Jin, Q. Kuang, Z.-X. Xie, S.-Y. Xie, R.-B. Huang, and L.-S. Zheng, *J. Mater. Chem.*, **19**, 6154 (2009).
46. Z. Xiao, Y. Xia, Z. Ren, Z. Liu, G. Xu, C. Chao, X. Li, G. Shen, and G. Han, *J. Mater. Chem.*, **22**, 20566 (2012).
47. S. Gustafsson, A. Fornara, K. Petersson, C. Johansson, M. Muhammed, and E. Olsson, *Cryst. Growth Des.*, **10**, 2278 (2010).
48. B. I. Kharisov, H. R. Dias, O. V. Kharissova, V. M. Jiménez-Pérez, B. O. Perez, and B. M. Flores, *RSC Adv.*, **2**, 9325 (2012).
49. L.-H. Shen, J.-F. Bao, D. Wang, Y.-X. Wang, Z.-W. Chen, L. Ren, X. Zhou, X.-B. Ke, M. Chen, and A.-Q. Yang, *Nanoscale*, **5**, 2133 (2013).
50. L. Zhang, W.-F. Dong, and H.-B. Sun, *Nanoscale*, **5**, 7664 (2013).
51. H. Zhang and G. Zhu, *Appl. Surf. Sci.*, **258**, 4952 (2012).
52. M. Miyauchi, T. J. Simmons, J. Miao, J. E. Gagner, Z. H. Shriver, U. Aich, J. S. Dordick, and R. J. Linhardt, *ACS Appl. Mater. Interfaces*, **3**, 1958 (2011).
53. Y. Si, T. Ren, B. Ding, J. Yu, and G. Sun, *J. Mater. Chem.*, **22**, 4619 (2012).
54. H. Green, T. Fox, and A. Scallan, *Pulp Pap. Canada*, **83**, 39 (1982).
55. R. Marchessault, P. Rioux, and L. Raymond, *Polymer*, **33**, 4024 (1992).
56. P. Rioux, S. Ricard, and R. Marchessault, *J. Pulp Pap. Sci.*, **18**, J39 (1992).
57. S. Zakaria, B. Ong, and T. Van de Ven, *Colloid Surf. A-Physicochem. Eng. Asp.*, **251**, 31 (2004).
58. S. Zakaria, B. Ong, S. Ahmad, M. Abdullah, and T. Yamauchi, *Mater. Chem. Phys.*, **89**, 216 (2005).
59. C. H. Chia, S. Zakaria, K. Nguyen, and M. Abdullah, *Ind. Crops Prod.*, **28**, 333 (2008).
60. L. Raymond, J.-F. Revol, D. Ryan, and R. Marchessault, *Chem. Mater.*, **6**, 249 (1994).
61. J. A. Carrazana-García, M. Lopez-Quintela, and J. Rivas-Rey, *Colloid Surf. A-Physicochem. Eng. Asp.*, **121**, 61 (1997).
62. D. Kim, Y. Zhang, W. Voit, K. Rao, and M. Muhammed, *J. Magn. Magn. Mater.*, **225**, 30 (2001).
63. H. Pardoe, W. Chua-Anusorn, T. G. S. Pierre, and J. Dobson, *J. Magn. Magn. Mater.*, **225**, 41 (2001).
64. J. Chatterjee, Y. Haik, and C.-J. Chen, *J. Magn. Magn. Mater.*, **257**, 113 (2003).
65. F. Katsuhisa, *Tappi J.*, **57**, 416 (2003).
66. F. Katsuhisa and M. Masaaki, *Tappi J.*, **57**, 556 (2003).
67. J. Wang, K. Zhang, Z. Peng, and Q. Chen, *J. Cryst. Growth*, **266**, 500 (2004).
68. J. Giri, S. G. Thakurta, J. Bellare, A. K. Nigam, and D. Bahadur, *J. Magn. Magn. Mater.*, **293**, 62 (2005).
69. C. Chia, S. Zakaria, S. Ahamd, M. Abdullah, and S. M. Jani, *Am. J. App. Sci.*, **3**, 1750 (2006).
70. A. C. Small and J. H. Johnston, *J. Colloid Interface Sci.*, **331**, 122 (2009).
71. R. F. Munawar, S. Zakaria, S. Radiman, C.-C. Hua, M. Abdullah, and T. Yamauchi, *Sains Malaysiana*, **39**, 593 (2010).
72. J. Wiener, S. Shahidi, and M. Goba, *Optics & Laser Technology*, **45**, 147 (2013).
73. L. Ai, C. Zhang, F. Liao, Y. Wang, M. Li, L. Meng, and J. Jiang, *J. Hazard. Mater.*, **198**, 282 (2011).
74. I. Langmuir, *J. Am. Chem. Soc.*, **38**, 2221 (1916).
75. H. M. F. Freundlich, *Z. Phys. Chem.*, **57A**, 385 (1906).
76. S. Lagergren, *Kungliga Svenska Vetenskapsakademiens. Handlingar*, **24**, 1 (1898).
77. G. Blanchard, M. Maunaye, and G. Martin, *Water Res.*, **18**, 1501 (1984).
78. Y.-S. Ho, "Absorption of Heavy Metals from Waste Streams by Peat", PhD. Thesis, University of Birmingham, 1995.
79. Y.-S. Ho, *Water Res.*, **40**, 119 (2006).
80. S. K. Milonjić, *J. Serb. Chem. Soc.*, **72**, 1363 (2007).
81. S. K. Milonjić, *J. Environ. Radioact.*, **100**, 921 (2009).
82. H. N. Tran, S.-J. You, and H.-P. Chao, *J. Environ. Chem. Eng.*, **4**, 2671 (2016).
83. J. A. R. Guivar, A. I. Martínez, A. O. Anaya, L. D. L. S. Valladares, L. L. Félix, and A. B. Dominguez, *Adv. Nanopart.*, **3**, 114 (2014).
84. O. Horner, S. Neveu, S. de Montredon, J.-M. Siaugue, and V. Cabuil, *J. Nanopart. Res.*, **11**, 1247 (2009).
85. W. Wu, X. Xiao, S. Zhang, T. Peng, J. Zhou, F. Ren, and C. Jiang, *Nanoscale Res. Lett.*, **5**, 1474 (2010).
86. T. Hyeon, S. S. Lee, J. Park, Y. Chung, and H. B. Na, *J. Am. Chem. Soc.*, **123**, 12798 (2001).
87. D. De Faria, S. Venâncio Silva, and M. De Oliveira, *J. Raman Spectrosc.*, **28**, 873 (1997).
88. M. Hanesch, *Geophys. J. Int.*, **177**, 941 (2009).
89. K. Woo, J. Hong, S. Choi, H.-W. Lee, J.-P. Ahn, C. S. Kim, and S. W. Lee, *Chem. Mater.*, **16**, 2814 (2004).
90. Z. Jing, *Mater. Lett.*, **60**, 2217 (2006).
91. M. D. P. Morales, S. Veintemillas-Verdaguer, M. Montero, C. Serna, A. Roig, L. Casas, B. Martinez, and F. Sandiumenge, *Chem. Mater.*, **11**, 3058 (1999).
92. F. Ferrero, *Clean Technol. Environ. Policy*, **17**, 1907 (2015).
93. S. Giri, N. Das, and G. Pradhan, *Colloid Surf. A-Physicochem. Eng. Asp.*, **389**, 43 (2011).
94. W. Zhang, F. Liang, C. Li, L.-G. Qiu, Y.-P. Yuan, F.-M. Peng, X. Jiang, A.-J. Xie, Y.-H. Shen, and J.-F. Zhu, *J. Hazard. Mater.*, **186**, 984 (2011).

95. G. Crini and P.-M. Badot, "Sorption Processes and Pollution: Conventional and Non-conventional Sorbents for Pollutant Removal from Wastewaters", Presses Univ. Franche-Comté, 2010.
96. K. R. Hall, L. C. Eagleton, A. Acrivos, and T. Vermeulen, *Ind. Eng. Chem. Fundam.*, **5**, 212 (1966).
97. B. S. Inbaraj and B. Chen, *Bioresour. Technol.*, **102**, 8868 (2011).
98. J.-F. Liu, Z.-S. Zhao, and G.-B. Jiang, *Environ. Sci. Technol.*, **42**, 6949 (2008).
99. J. Wang, S. Zheng, Y. Shao, J. Liu, Z. Xu, and D. Zhu, *J. Colloid Interface Sci.*, **349**, 293 (2010).
100. C. Yang, J. Du, Q. Peng, R. Qiao, W. Chen, C. Xu, Z. Shuai, and M. Gao, *J. Phys. Chem. B*, **113**, 5052 (2009).
101. J. de Souza Macedo, N. B. da Costa Júnior, L. E. Almeida, E. F. da Silva Vieira, A. R. Cestari, I. de Fátima Gimenez, N. L. V. Carreño, and L. S. Barreto, *J. Colloid Interface Sci.*, **298**, 515 (2006).
102. D. Pathania, S. Sharma, and P. Singh, *Arabian J. Chem.*, **10**, S1445 (2017).
103. R. Hazzaa and M. Hussein, *Environ. Technol. Innov.*, **4**, 36 (2015).
104. S. Naeem, V. Baheti, J. Militky, J. Wiener, P. Behera, and A. Ashraf, *Fiber. Polym.*, **17**, 1245 (2016).
105. S. Naeem, V. Baheti, J. Wiener, and J. Marek, *J. Text. Inst.*, **108**, 803 (2017).
106. J.-L. Gong, B. Wang, G.-M. Zeng, C.-P. Yang, C.-G. Niu, Q.-Y. Niu, W.-J. Zhou, and Y. Liang, *J. Hazard. Mater.*, **164**, 1517 (2009).
107. S. Giri, N. Das, and G. Pradhan, *Powder Technol.*, **214**, 513 (2011).
108. C. Păcurariu, O. Paşka, R. Ianoş, and S. G. Muntean, *Clean Technol. Environ. Policy*, **18**, 705 (2016).